QUANTUM SENSING

Nanoscale covariance magnetometry with diamond quantum sensors

Jared Rovny[1], Zhiyang Yuan[1], Mattias Fitzpatrick[1]†, Ahmed I. Abdalla[1]‡, Laura Futamura[1]§, Carter Fox[2], Matthew Carl Cambria[2], Shimon Kolkowitz[2], Nathalie P. de Leon[1]*

Nitrogen vacancy (NV) centers in diamond are atom-scale defects that can be used to sense magnetic fields with high sensitivity and spatial resolution. Typically, the magnetic field is measured by averaging sequential measurements of single NV centers, or by spatial averaging over ensembles of many NV centers, which provides mean values that contain no nonlocal information about the relationship between two points separated in space or time. Here, we propose and implement a sensing modality whereby two or more NV centers are measured simultaneously, and we extract temporal and spatial correlations in their signals that would otherwise be inaccessible. We demonstrate measurements of correlated applied noise using spin-to-charge readout of two NV centers and implement a spectral reconstruction protocol for disentangling local and nonlocal noise sources.

Correlated phenomena play a central role in condensed matter physics and have been studied in many contexts, including phase transitions (*1*, *2*), many-body interactions and entanglement (*3*, *4*), and magnetic ordering (*5*, *6*), as well as in the context of fluctuating electromagnetic fields, where two-point correlators are central to characterizing field statistics (*7*, *8*). Recent efforts toward improving quantum devices have also explored correlated noise in superconducting quantum interference devices (*9*) and qubits (*10*–*12*). Nitrogen vacancy (NV) centers in diamond are a promising sensing platform for detecting correlations because they are robust, noninvasive, and capable of measuring weak signals with nanoscale resolution (*13*). These advantages have made them a useful tool for studying many condensed matter systems, including magnetic systems such as two-dimensional (2D) van der Waals materials (*14*, *15*), magnons (*16*), and skyrmions (*17*, *18*); and transport phenomena such as Johnson noise (*19*), hydrodynamic flow (*20*–*22*), and electron-phonon interactions in graphene (*23*). These applications are powerful but have so far been limited to signals that are averaged over space or time—more information is potentially available by studying spatial and temporal correlations in the system. Advances in nanoscale spectroscopy have already been made by studying correlations from a single NV center at different points in time (*24*–*26*), where temporal correlations are calculated between subsequent measurements before signal averaging. Here, we extend this technique to measuring correlations in both space and time between individual measurements with pairs of NV centers before signal averaging; measuring correlated dynamics between two different NV centers provides simultaneous information at length scales ranging from the diffraction limit to the full field of view (~0.1- to 100-μm length scales) and at two different sensing times limited only by the experimental clock cycle (~1-ns resolution). Measurements of spatiotemporal correlations at these length and time scales would provide useful information about the dynamics of the target system, including the electron mean free path, signatures of hydrodynamic flow (*27*), or the microscopic nature of local NV center noise sources such as surface spins (*28*, *29*).

Determining correlations between NV centers

We consider two NV centers that do not directly interact with each other but experience a shared classical magnetic field, whose amplitude is correlated at the locations of the two NV centers (Fig. 1A). Each NV center also sees a distinct local magnetic field that is uncorrelated between the two locations. These fields are detected using a Ramsey-type experiment that addresses the $m_s = 0$ and $m_s = +1$ (or –1) spin sublevels of the NV center (referred to as states 0 and 1, respectively) (Fig. 1, B to D). After many repeated measurements, we accumulated a list of signals $S_1 = \{s_{1,i}\}$ and $S_2 = \{s_{2,i}\}$ from NV1 and NV2, respectively, where s is the number of photons detected in a single experiment and $i = 1 \ldots N$ indexes the N total experiments.

Though similar to a typical Ramsey-type variance detection sequence (*30*), we emphasize two modifications for covariance detection. First, despite detecting zero-mean noise, we chose a final pulse that is 90° out of phase with the initial pulse, such that for high-frequency noise detection, the final spin state is equally likely to be 0 or 1 (Fig. 1, B and C), which maximizes our sensitivity to correlations. This is not done in conventional noise detection using variance magnetometry, because straightforward signal averaging would then always produce the same result $\langle m_{s_i} \rangle = 0.5$. Second, we did not compute the average value of this signal but rather computed the shot-to-shot cross-correlation between the raw signals S_1 and S_2 (Fig. 1D).

Whereas conventional variance measurements provide spectral densities with no spatial information (top row of Fig. 1E), the addition of covariance information allows us to identify which spectral components are common between two NV centers and which are specific to each (bottom row of Fig. 1E). Throughout this work, we focus on the measured Pearson correlation $r = \mathrm{Cov}(S_1, S_2)/(\sigma_1\sigma_2)$, where Cov is the covariance and σ_1 and σ_2 are the standard deviations of S_1 and S_2.

Experimental implementation of covariance measurements

To demonstrate our protocol, we used an external radiofrequency coil or stripline to apply a global, random phase ac signal to two shallow NV centers ~10 nm from the diamond surface. Here, the two NV centers share the same magnetic resonance frequency, so that all microwave pulses address both. They are spatially resolved, which allows for separate excitation and readout using two independent optical paths (*31*). To boost the sensitivity of our readout, we used a simultaneous spin-to-charge conversion (SCC) protocol (*32*, *33*) on each NV center separately. We used an XY8 sensing protocol for each NV center to maximize sensitivity to the applied ac signal (*34*) (Fig. 2A). We observed correlations that are maximized when the interpulse spacing matches the frequency of the global signal (blue circles in Fig. 2B). The correlations are apparent in the photon count statistics [bottom panel (ii) of Fig. 2B]; when one or more photons are detected from NV1, we observed a higher likelihood of also detecting a photon from NV2. To confirm that we were indeed detecting correlations in the spin state of the NV centers rather than spurious technical correlations (*31*), we could also initialize the two NV centers on opposite sides of the Bloch sphere before applying the XY8 sequence (Fig. 2A). The phase accumulation step then results in a final state that is anticorrelated between the two NV centers (red squares in Fig. 2B).

The sensitivity of a covariance measurement differs from that of a traditional magnetometry measurement because it requires simultaneous signals from two NV centers. Assuming that the detected phases are statistically even, as for a noisy or random-phase signal, we find (*31*) the Pearson correlation

$$r = \frac{e^{-[\tilde{\chi}_1(t_1) + \tilde{\chi}_2(t_2)]}}{\sigma_{R_1}\sigma_{R_2}} \left\langle \sin\left[\phi_{C_1}(t_1)\right] \sin\left[\phi_{C_2}(t_2)\right] \right\rangle \quad (1)$$

---

[1] Department of Electrical and Computer Engineering, Princeton University, Princeton, NJ 08544, USA.
[2] Department of Physics, University of Wisconsin–Madison, Madison, WI 53706, USA.
***Corresponding author. Email: npdeleon@princeton.edu**
†Present address: Thayer School of Engineering, Dartmouth College, Hanover, NH 03755, USA.
‡Present address: Department of Electrical Engineering, Stanford University, Stanford, CA 94305, USA.
§Present address: Department of Physics, Stanford University, Stanford, CA 94305, USA.

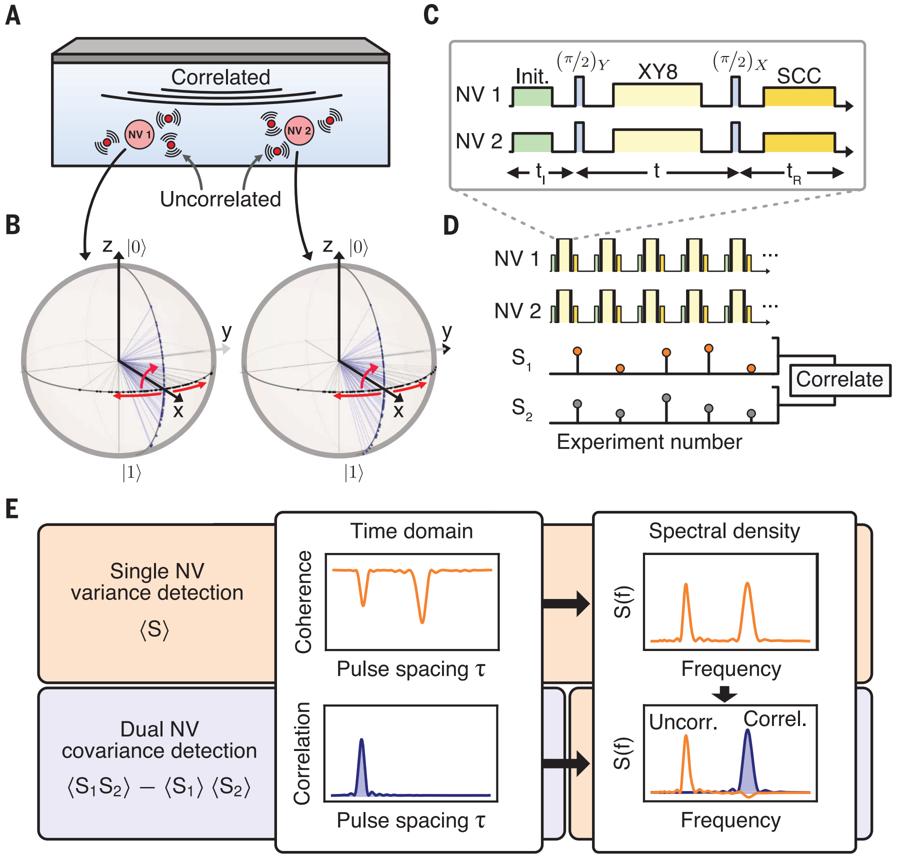

Fig. 1. Covariance noise sensing. (**A**) Diagram of a diamond with two near-surface NV centers that are experiencing uncorrelated local fields and a correlated common field. (**B**) Bloch sphere representations of each qubit state during sensing, with the states prepared along x followed by a phase accumulation that will be different in each experiment, resulting in a distribution of phases. At the end of each experiment, a final $\pi/2$ pulse maps these phases to populations. (**C** and **D**) Pulse sequence diagrams showing the sensing (XY8) and measurement (SCC) sequence for each NV center. The measurement is repeated many times, retaining the photon counts from each measurement without signal averaging; we instead measured the correlation between the resulting lists S_i. (**E**) Using conventional detection of single NV centers (top row), the coherence decay gives access to the noise spectral density $S(f)$ but provides no spatial information. Covariance magnetometry measuring two NV centers (bottom row) provides information about which spectral features are correlated and which are uncorrelated.

where the subscripts 1 and 2 denote NV1 and NV2, respectively; the decoherence function $\tilde{\chi}_{1,2}(t)$ describes the "typical" coherence decay of the NV centers due to the local fields (*35*); $\phi_{C_{1,2}}$ are the phases accumulated by the NV centers due to the correlated field; and the readout noise $\sigma_{R_{1,2}} = \sqrt{1+2(\alpha_0+\alpha_1)/(\alpha_0-\alpha_1)^2}$ characterizes the fidelity of a photon-counting experiment with mean detected photon numbers α_0 and α_1 for spin states 0 and 1, respectively (*30*). For thresholding, the readout noise instead depends on the fidelity of the spin-state assignment. Readout noise may be generalized to include non-Poisson statistics that result from errors in charge-state initialization or ionization (*31*).

Note that the detectable correlation depends quadratically on the readout noise, which makes readout fidelity especially important for detecting correlations; this key fact is implicit in prior calculations of single-NV center two-point correlators derived in the context of repeated weak measurements (*25*). This may be intuitively understood from Fig. 2C, which shows the raw photon counts for conventional versus SCC readout methods. Using conventional readout, only ~0.01 photons are detected per measurement, such that detecting simultaneous counts from both NV centers is extremely unlikely. Using SCC readout substantially increases our ability to detect coincident events and has a greater effect on covariance measurements than on conventional single–NV center measurements. From the independently measured values for each term on the right-hand side of Eq. 1 (*31*), we expect the detectable correlation in our experiment to be approximately bounded by $r \approx 0.01$, in good agreement with the maximum correlation $r \approx 0.008$ that we detect here (Fig. 2B). The remaining discrepancy is likely due to experimental imperfections such as sample drift or pulse miscalibration over time.

Because readout noise plays an amplified role in covariance detection, covariance measurements can become prohibitively long without optimizing sensitivity, for which we require a detailed understanding of the signal-to-noise ratio (SNR). The sensitivity (minimum noise amplitude $\sigma_{B_{\min}}$ with SNR = 1) of an experiment that detects Gaussian noise is given by (*31*)

$$\sigma^2_{B,\min} = \frac{-\pi\cdot\mathrm{Hz}}{4{\gamma_e}^2 t}\ln\left(1-\frac{2{\sigma_R}^2 e^{2t/T_2}}{\sqrt{T/(t+t_R)}}\right) \quad (2)$$

where γ_e is the electron gyromagnetic ratio, t is the phase integration time, T_2 is the coherence time, t_R is the readout time, and $T \approx (t + t_R)N$ is the total experiment time ignoring initialization. This is shown in the bottom graph of Fig. 2C for three different readout methods: conventional (σ_R = 35), SCC (σ_R = 4), and single-shot readout with perfect fidelity (σ_R = 1), which is ultimately limited by quantum projection noise. Achieving an SNR equal to 1 for these three scenarios when σ_B = 1 nT requires total experiment times on the order of 300 hours, 3 hours, and 10 s, respectively. Whereas detecting correlations is extremely inefficient using conventional readout, enhanced readout protocols like SCC (*32*, *36*) allow for substantially lower readout noise, making covariance magnetometry possible to implement in practice.

Disentangling correlated and uncorrelated noise sources

Detecting cross-correlations in pure noise reveals previously hidden information about the spatial structure of the noise, which we now demonstrate using two NV centers that sense both local and nonlocal magnetic fields. We first measured the spectral density $S(f)$, where f is frequency, using a conventional variance magnetometry measurement of two different NV centers (Fig. 3A, top). These individual spectra reveal that there are two frequencies where signals are seen by both NV centers but cannot provide simultaneous nonlocal spatial information about that signal. Using covariance magnetometry over the same frequency range (Fig. 3A, bottom) shows only the higher-frequency feature, which clearly reveals that the higher-frequency feature is caused by a noise signal common to each NV center, whereas the lower-frequency feature is instead caused by local noise sources specific to each NV center.

This ability to distinguish correlated and uncorrelated features enables spatially resolved spectral decomposition, which allows us to distinguish spectral components that are shared from those that are local. For phases that are

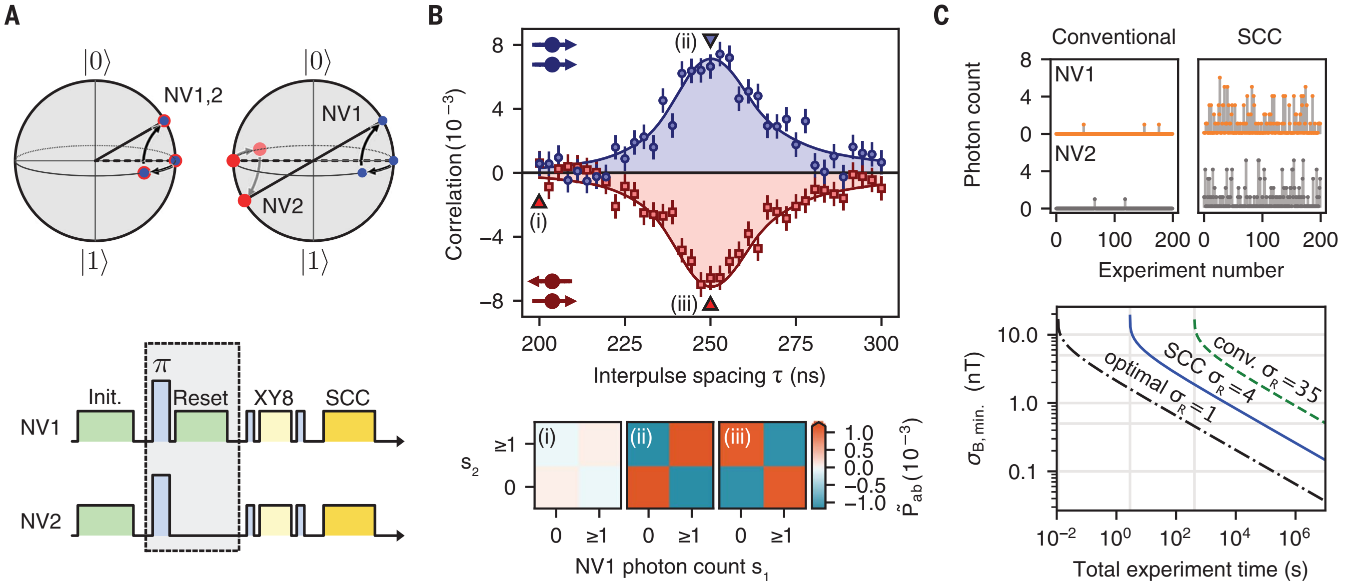

Fig. 2. Detecting correlations and anticorrelations. (**A**) Pulse sequence and final Bloch sphere mapping for correlation (top left) or anticorrelation (top right) measurements using global microwave control. For anticorrelations, an extra π pulse and spatially selective NV polarization optical pulse ("reset") are added during initialization (bottom, gray box). (**B**) Correlation detected from a 2-MHz ac signal whose phase is randomized with 1-MHz bandwidth Gaussian noise. The measured correlations are positive when the NV centers are initialized parallel to one another (blue circles) and negative when they are initialized antiparallel to one another (red squares). Lines indicate the predicted correlation shape (*31*). Raw photon count statistics (bottom) taken from the marked data points in the top panel show no correlation (i), positive correlation (ii), or negative correlation (iii), where the color indicates the joint detection probability $\tilde{P}_{ab} \equiv P(s_1 = a, s_2 = b) - P(s_1 = a)P(s_2 = b)$. (**C**) Comparison of shot-to-shot photon counts during averaging for conventional readout (top left) and SCC readout (top right). Minimum magnetic field amplitude to detect correlations with SNR = 1 for Gaussian noise is shown at the bottom. Here, we have assumed T_2 = 100 μs and the phase integration time $t = T_2/2$ = 50 μs, as well as a readout time of 300 ns for conventional readout and 1 ms for SCC and optimal readout. Initialization time was ignored. The horizontal and vertical gray lines are guides to the eye.

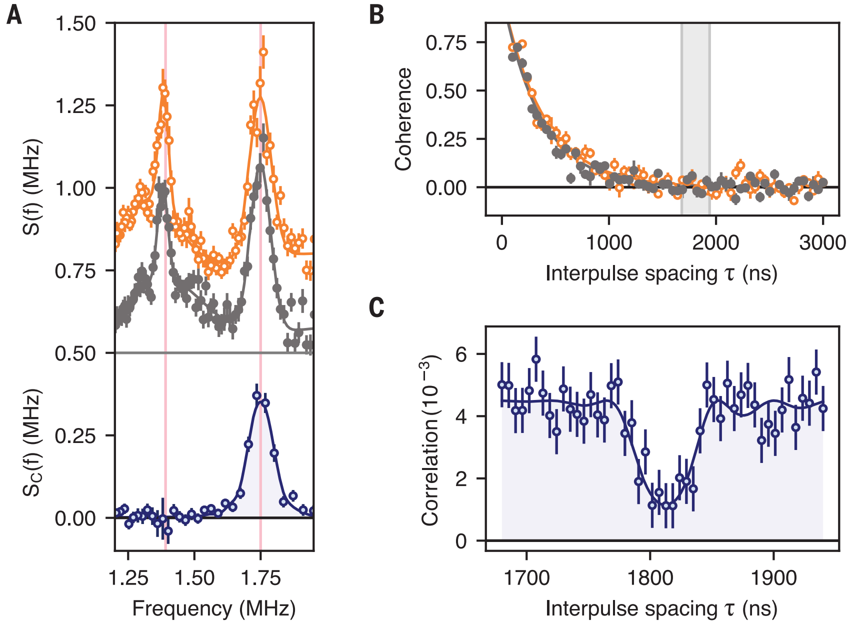

Fig. 3. Disentangling correlated and uncorrelated signals. (**A**) Single-NV noise spectra derived from conventional XY8 variance magnetometry (top) of two NV centers (orange open markers and gray filled markers with Gaussian fit lines, arbitrarily offset). Each NV center detects signals at two common frequencies, but it is impossible to directly determine whether the sources are local or nonlocal. Spectral decomposition (bottom) using covariance magnetometry (Eq. 3) reveals that the higher-frequency peak is caused by a shared noise source. Here, the shared noise feature is engineered using an applied global 1.75-MHz ac signal, whereas the local feature is caused by the ^{15}N nuclear spin intrinsic to each NV center. The line indicates the predicted correlation shape. The light red vertical lines indicate the expected peak locations (*31*). (**B**) In a broadband correlated noise environment, the two NV centers rapidly decohere (orange open markers and gray filled markers). Lines are exponential fits. (**C**) Covariance magnetometry for evolution times indicated by the gray region in (B) reveals a dip in the Pearson correlation around τ = 1800 ns that arises from the uncorrelated ^{15}N nuclear spins intrinsic to each NV center. The line indicates the predicted correlation shape. The broadband noise is correlated, which allows for the observation of spectral features from local signals even at evolution times beyond the coherence time of both NV centers.

Gaussian-distributed or small ($\phi \ll \pi$), we can find (*31*) the correlated noise spectrum $S_C(f)$ if we have access to both the two-NV correlation r as well as each NV center's coherence decay $C_i(t) = e^{-\chi(t)}$ [note that $C_i(t)$ includes both the correlated and uncorrelated noise sources]:

$$S_C(f) = \frac{\pi}{2t}\sinh^{-1}\left(\frac{{\sigma_R}^2 r}{C_1(t)C_2(t)}\right) \qquad (3)$$

where $t = n/(2f)$ and n is the total number of applied XY8 pulses. This equation is used to obtain the correlated spectrum from the measured correlation and single–NV center coherence decays, as shown in Fig. 3A. The

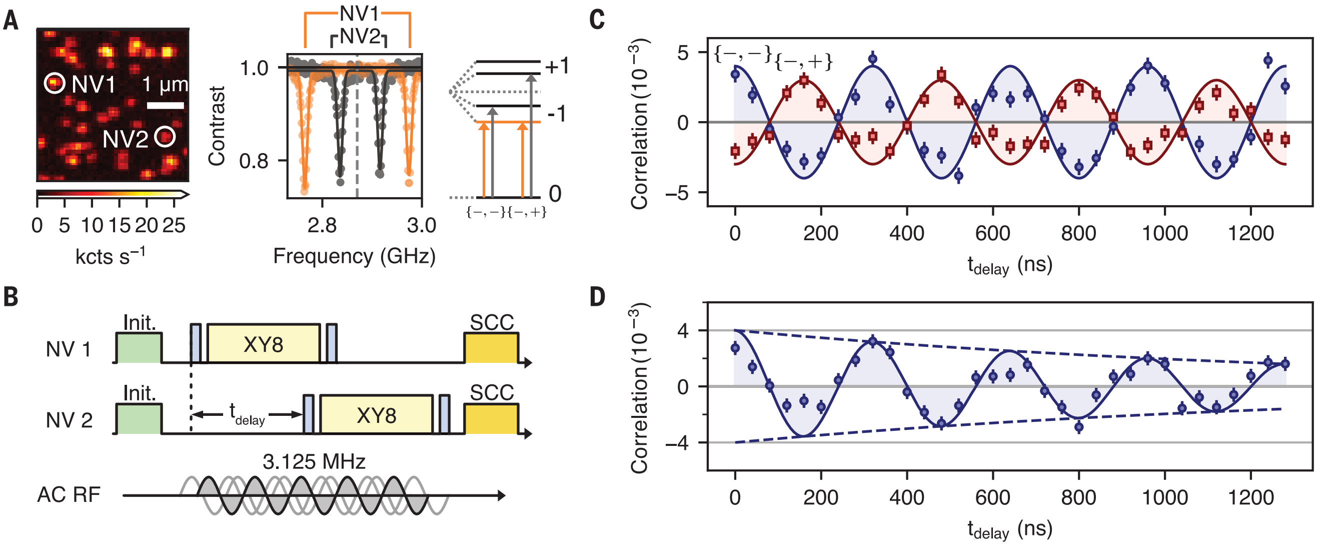

Fig. 4. Temporal structure in correlations using independent control. (**A**) Confocal image showing the two NV centers used for these experiments (left). Optically detected magnetic resonance spectrum (middle) showing optical contrast as a function of microwave drive frequency displays two distinct sets of transitions corresponding to NV1 and NV2, with assignments (right). The NV centers are driven independently on either the (0, −1) transitions for both NVs, labeled {−, −}, or the (0, −1) and (0, +1) transitions for NV1 and NV2, respectively, labeled {−, +}. (**B**) Diagram of the pulse sequence used to probe temporal correlations. After initialization, the start of the XY8 pulse sequence applied to NV2 is delayed by time t_{delay} from the start of the pulses on NV1. A f_0 = 3.125 MHz global ac signal is applied, making the resonant XY8 interpulse spacing τ = 160 ns. (**C**) Correlations for the case in which the NV centers are addressed on the same transitions ({−, −}, blue circles) oscillate as a function of t_{delay} at the ac signal frequency of 3.125 MHz. The correlations invert (red squares) when the two NV centers are addressed on different transitions ({−, +}), because they now accumulate opposite phases for the same signal. (**D**) With added phase noise, the time-domain dephasing of the ac signal is resolvable, despite having a short coherence time (less than 2 μs) compared with the XY8 sequence time.

local spectrum for each NV center $S_{L_{1,2}}(f)$ may also be found from each individual NV center's total spectrum $S_{L_{1,2}}(f) = S_{1,2}(f) - S_C(f)$.

So far, we have analyzed the case where shared and local features are spectrally resolved, but an interesting scenario arises when a shared signal decoheres each NV center at frequencies coincident with local noise sources. To probe this case, we applied a global broadband Gaussian noise signal, decohering both NV centers while inducing broadband correlations in their phases (Fig. 3, B and C). Beyond the coherence time of each NV center, conventional variance detection cannot reveal any information (gray region in Fig. 3B). However, covariance magnetometry (Fig. 3C) measures the broadband correlation in the random phases of the decohered NV centers; this correlation will dip if either NV center interacts with a local noise source in its vicinity, because the local signal induces a phase that is specific to that NV center. The covariance magnetometry spectrum therefore reveals a feature that is hidden in the single-NV spectra.

Temporal structure of correlations

Covariance magnetometry also enables measurements of the temporal structure of the two-point correlator $\langle B(r_1, t_1)B(r_2, t_2)\rangle$ separated in time as well as space for short time scales where $t_2 - t_1 < t + t_R$, which is not possible with single–NV center correlation measurements (*24*–*26*). To perform this measurement, independent control of each NV center is required. We accomplished this by choosing two NV centers with different orientations at low magnetic fields (Fig. 4A), such that the 0→−1 transition of the NV center that is aligned with the magnetic field is detuned by 70 MHz from that of the misaligned NV center. We then offset the beginning of the XY8 sequence applied to NV2 by time t_{delay} (Fig. 4B) and measured an applied ac field at frequency f_0 = 3.125 MHz. As we swept t_{delay}, the correlations oscillated at frequency f_0 (Fig. 4C), as expected for a random-phase ac signal (*26*, *37*). Independent control also allowed us to simultaneously address opposite spin transitions for each NV center (Fig. 4A, right). Because the two NV centers then accumulate opposite phases from the ac field, we observed anticorrelations with the same frequency (red squares in Fig. 4C).

Because the two NV centers are manipulated independently, there are no fundamental constraints on the length of t_{delay}. This allowed us to directly measure time-domain structure on the nanosecond time scale at two points in space, despite using π pulses with 60-ns duration. When we measured the correlations between two NV centers experiencing a shared ac signal with added phase noise (Fig. 4D), we could directly resolve the temporal structure of the ac signal despite its short coherence time of less than 2 μs, without making use of spectral deconvolution. We emphasize that this technique is very general and is thus applicable to any time-varying signal with a nonzero correlation time that can be detected with NV centers. Correlations will remain detectable on the time scale of the underlying signal correlation time, even when the signal phase is completely random from one experiment to the next (as in Fig. 3C).

Concluding remarks

Our demonstration of simultaneous control and readout of two spatially resolved NV centers shows that nanoscale magnetometry of two-point spatiotemporal field correlators that would normally be discarded using conventional NV center magnetometry is possible. Spatiotemporal correlations of any signal that can be imprinted as a phase on the NV centers can be sensed with this technique, provided that the statistics of the signal remain sufficiently stationary over the course of the experiment. Our approach has many potential applications; measurements of these two-point correlators can reveal the underlying length and time scales of fluctuating electromagnetic fields near surfaces (*7*, *8*), which provides information about nonequilibrium transport dynamics (*38*) and condensed matter phenomena like magnetic ordering in low-dimensional systems (*5*, *15*). For example, there has been considerable recent interest in studying hydrodynamic flow in 2D materials (*20*–*22*), but it is challenging to directly observe the hydrodynamic transition—covariance noise sensing could provide new quantitative information about these dynamics. Also, magnetic excitations such as magnons can have micron-scale dynamics, a natural length scale for covariance magnetometry with pairs of NV centers. Future extensions of the current demonstration include using photonic structures to improve photon collection efficiency (*33*), applying different pulse sequences to each NV center to probe the correlations between signals at different frequencies or phases (*39*), measuring more NV centers to measure higher-order joint cumulants (*31*), and using detector arrays to perform simultaneous readout of many pairs of NV centers.

REFERENCES AND NOTES

1. H. Bernien *et al.*, *Nature* **551**, 579–584 (2017).
2. J. Zhang *et al.*, *Nature* **551**, 601–604 (2017).
3. X.-L. Deng, D. Porras, J. I. Cirac, *Phys. Rev. A* **72**, 063407 (2005).
4. M. L. Baez *et al.*, *Proc. Natl. Acad. Sci. U.S.A.* **117**, 26123–26134 (2020).
5. A. Mazurenko *et al.*, *Nature* **545**, 462–466 (2017).
6. J. Simon *et al.*, *Nature* **472**, 307–312 (2011).
7. V. N. Premakumar, M. G. Vavilov, R. Joynt, *Quantum Sci. Technol.* **3**, 015001 (2017).
8. K. Agarwal *et al.*, *Phys. Rev. B* **95**, 155107 (2017).
9. S. Gustavsson *et al.*, *Phys. Rev. B* **84**, 014525 (2011).
10. C. D. Wilen *et al.*, *Nature* **594**, 369–373 (2021).
11. U. von Lüpke *et al.*, *PRX Quantum* **1**, 010305 (2020).
12. P. Szańkowski, M. Trippenbach, Ł. Cywiński, *Phys. Rev. A* **94**, 012109 (2016).
13. F. Casola, T. van der Sar, A. Yacoby, *Nat. Rev. Mater.* **3**, 17088 (2018).
14. Q.-C. Sun *et al.*, *Nat. Commun.* **12**, 1989 (2021).
15. L. Thiel *et al.*, *Science* **364**, 973–976 (2019).
16. E. Lee-Wong *et al.*, *Nano Lett.* **20**, 3284–3290 (2020).
17. A. Jenkins *et al.*, *Phys. Rev. Mater.* **3**, 083801 (2019).
18. Y. Dovzhenko *et al.*, *Nat. Commun.* **9**, 2712 (2018).
19. S. Kolkowitz *et al.*, *Science* **347**, 1129–1132 (2015).
20. M. J. H. Ku *et al.*, *Nature* **583**, 537–541 (2020).
21. U. Vool *et al.*, *Nat. Phys.* **17**, 1216–1220 (2021).
22. A. Jenkins *et al.*, *Phys. Rev. Lett.* **129**, 087701 (2022).
23. T. I. Andersen *et al.*, *Science* **364**, 154–157 (2019).
24. J. M. Boss, K. S. Cujia, J. Zopes, C. L. Degen, *Science* **356**, 837–840 (2017).
25. M. Pfender *et al.*, *Nat. Commun.* **10**, 594 (2019).
26. A. Laraoui *et al.*, *Nat. Commun.* **4**, 1651 (2013).
27. L. Levitov, G. Falkovich, *Nat. Phys.* **12**, 672–676 (2016).
28. B. L. Dwyer *et al.*, arXiv:2103.12757 [quant-ph] (2021).
29. S. Sangtawesin *et al.*, *Phys. Rev. X* **9**, 031052 (2019).
30. J. M. Taylor *et al.*, *Nat. Phys.* **4**, 810–816 (2008).
31. See supplementary materials.
32. B. J. Shields, Q. P. Unterreithmeier, N. P. de Leon, H. Park, M. D. Lukin, *Phys. Rev. Lett.* **114**, 136402 (2015).
33. J. F. Barry *et al.*, *Rev. Mod. Phys.* **92**, 015004 (2020).
34. T. Gullion, D. B. Baker, M. S. Conradi, *J. Magn. Reson.* **89**, 479–484 (1990).
35. Ł. Cywiński, R. M. Lutchyn, C. P. Nave, S. Das Sarma, *Phys. Rev. B* **77**, 174509 (2008).
36. D. A. Hopper, H. J. Shulevitz, L. C. Bassett, *Micromachines* **9**, 437 (2018).
37. C. L. Degen, F. Reinhard, P. Cappellaro, *Rev. Mod. Phys.* **89**, 035002 (2017).
38. P. E. Dolgirev *et al.*, *Phys. Rev. B* **105**, 024507 (2022).
39. P. Szańkowski, G. Ramon, J. Krzywda, D. Kwiatkowski, Ł. Cywiński, *J. Phys. Condens. Matter* **29**, 333001 (2017).
40. J. Rovny *et al.*, Nanoscale covariance magnetometry with diamond quantum sensors, *Harvard Dataverse* (2022); https://doi.org/10.7910/DVN/XMEIHR.

ACKNOWLEDGMENTS

We acknowledge helpful conversations with A. Burgers, S. Gopalakrishnan, and J. Thompson. **Funding:** This work was funded by NSF CAREER grant DMR-1752047; the Princeton Catalysis Initiative; the US Department of Energy, Office of Science, Office of Basic Energy Sciences, under award no. DE-SC0018978; the US Department of Energy Office of Science National Quantum Information Science Research Centers; a Princeton Quantum Initiative Postdoctoral Fellowship (J.R.); and the Intelligence Community Postdoctoral Research Fellowship Program by the Oak Ridge Institute for Science and Education (ORISE) through an interagency agreement between the US Department of Energy and the Office of the Director of National Intelligence (ODNI) (M.F.). **Author contributions:** Theoretical framework: J.R., M.F., A.I.A., C.F., M.C.C., S.K., N.P.d.L.; Experiment: J.R., Z.Y., L.F.; Sensing technique, experimental design, data analysis: J.R., C.F., M.C.C., S.K., N.P.d.L.; Writing: J.R., C.F., M.C.C., S.K., N.P.d.L. **Competing interests:** The authors declare that they have no competing interests. **Data and materials availability:** All data needed to evaluate the conclusions in this paper are present in the paper or the supplementary materials and are publicly available at Harvard Dataverse (*40*).

SUPPLEMENTARY MATERIALS

science.org/doi/10.1126/science.ade9858
Materials and Methods
Figs. S1 and S2
References (*41*–*45*)

Submitted 20 September 2022; accepted 25 November 2022
10.1126/science.ade9858

Nanoscale covariance magnetometry with diamond quantum sensors

Jared Rovny, Zhiyang Yuan, Mattias Fitzpatrick, Ahmed I. Abdalla, Laura Futamura, Carter Fox, Matthew Carl Cambria,
Shimon Kolkowitz, and Nathalie P. de Leon

Science, **378** (6626), .
DOI: 10.1126/science.ade9858

Covariance magnetometry
Color defect centers in diamond, such as the nitrogen vacancy center effect, behave as miniature compass needles. Their optical signature is sensitive to local magnetic fields with nanoscale resolution. To date, these sensing modalities have been largely limited to detecting static magnetic fields or sensing an ensemble average, providing access to dynamical behavior only indirectly. Rovny *et al.* developed a theoretical framework and demonstrate a new sensing modality for detecting spatiotemporal correlations from simultaneous measurements of two nitrogen vacancy defect centers in diamond. Covariance measurements open a window for sensing spatiotemporal dynamics through nanoscale magnetometry. —ISO

Science (ISSN) is published by the American Association for the Advancement of Science. 1200 New York Avenue NW, Washington, DC 20005. The title *Science* is a registered trademark of AAAS.